

Multi-band Reconfigurable Holographic Surface Based ISAC Systems: Design and Optimization

Jingzhi Hu*, Zhe Chen[†], and Jun Luo*

*School of Computer Science and Engineering, Nanyang Technological University, Singapore,

[†]China-Singapore International Joint Research Institute and AIWiSe Technology Co., Ltd, Guangzhou, China.

Abstract—Metamaterial-based reconfigurable holographic surfaces (RHSs) have been proposed as novel cost-efficient antenna arrays, which are promising for improving the positioning and communication performance of integrated sensing and communications (ISAC) systems. However, due to the high frequency selectivity of the metamaterial elements, RHSs face challenges in supporting ultra-wide bandwidth (UWB), which significantly limits the positioning precision. In this paper, to avoid the physical limitations of UWB RHS while enhancing the performance of RHS-based ISAC systems, we propose a multi-band (MB) RHS based ISAC system. We analyze its positioning precision and propose an efficient algorithm to optimize the large number of variables in analog and digital beamforming. Through comparison with benchmark results, simulation results verify the efficiency of our proposed system and algorithm, and show that the system achieves 42% less positioning error, which reduces 82% communication capacity loss.

I. INTRODUCTION

Recently, metamaterial-based reconfigurable holographic surfaces (RHSs) have been proposed as novel cost-efficient antenna arrays, which possess high potential in improving the performance of wireless networks [1]. RHSs are characterized by their large number of densely arranged metamaterial antenna elements (*meta-elements*), which have smaller spatial intervals than half of their working wavelength [2]. Such dense placement enables RHSs to have strong manipulation capability for electromagnetic (EM) waves and can synthesize various beam forms through analog and digital (A&D) beamforming [3]. By leveraging this capability, a base station (BS) equipped with an RHS can focus transmitted signals towards users for communication enhancement.

To achieve this enhancement, the RHS-based BSs need to know the channel state information (CSI) or the positions of the users. However, the channel state estimation problem of the RHSs is highly complicated due to the large number of meta-elements lacking signal processing capability [4]. Alternatively, using the RHS, a BS can effectively positioning a target user and focus its beam towards it. This indicates that the RHS-based BSs are intrinsically fit for integrated sensing and communications (ISAC) in the sense that the communication can benefit from the positioning results obtained by the RHS.

In this regard, the performance of an RHS-based ISAC system is fundamentally influenced by its positioning precision. In literature, several works have considered the positioning aspect of RHS-based ISAC systems. In [3], the authors proposed a beamforming algorithm to simultaneously generate beams for communication and sensing purposes with high directional gains. In [5], the authors used RHS for target detection and obtained high accuracy with low cost and power consumption.

Additionally, given the essential similarity between reconfigurable intelligent surfaces (RISs) and RHSs, the positioning techniques for RIS-based systems have the potential to be applied in RHS-based systems¹. In [6], the authors utilized an RIS to generate distinguishable signals strength values for different locations to facilitate positioning. In [7], the authors proposed a SNR-based RIS configuration profile that increases the positioning precision.

However, in existing works, the fundamental limitation is that the signal bandwidths for positioning are not broad enough. This reduces the positioning precision, as the spatial resolution of positioning typically increases with the bandwidth [8]. Though the authors in [9] considered using ultra-wide-band (UWB) technique in RIS-based positioning systems, it is challenging to implement RIS or RHS that can support beamforming of UWB signals in practice, due to the high frequency selectivity of the reconfigurable meta-elements [1], [2].

In this paper, we propose the multi-band (MB) RHS-based ISAC system, where multiple uplink bands are utilized in a time-division duplex (TDD) manner to enhance the positioning precision and eventually leads to better communication capacity. The MB technique is a promising alternative of UWB [10]. As the feasibility of MB meta-element has been addressed in literature [11], the MB RHS becomes a promising solution to get around the bandwidth limitation and achieve high positioning precision. To fully exploit the strength of the proposed system, we propose a *position-then-transmit protocol* for the system. Based on the protocol, we establish the channel model of the system in a rich scattering environment. Then, we derive the positioning precision of the system in terms of the Cramer-Rao lower bound (CRLB) given the A&D beamforming of the RHS.

¹The main difference between RISs and RHSs is that RISs perform beamforming by reflecting signals, while RHSs radiate the signals themselves.

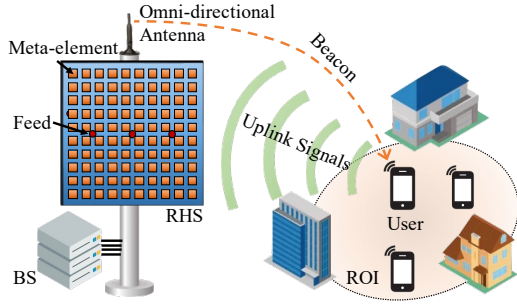


Fig. 1. MB RHS-based ISAC system

Nevertheless, as multiple bands are adopted, the large number of controlling variables in the A&D beamforming is further multiplied, which cannot be handled by conventional small-scale optimization algorithms efficiently. To handle this challenge, we derive a closed-form formula of the CRLB's gradient and then propose an efficient block coordinate descent (BCD) algorithm where the digital and analog beamforming variables are optimized alternately. Simulation results verify that with the proposed algorithm, the MB RHS-based system achieves lower CRLB in positioning, which leads to lower positioning error and much smaller communication capacity loss compared with benchmarks.

The rest of the paper is organized as follows. In Section II, we propose the system model, the protocol, and the channel model of the MB RHS-based ISAC system. In Section III, the CRLB of positioning is derived, and the problem for beamforming optimization is formulated. In Section IV, the gradients of CRLB are derived, and the algorithm to solve the formulated problem is designed. Simulation results are provided in Section V, and a conclusion is drawn in Section VI.

Notations: $(\cdot)^*$, $(\cdot)^T$, and $(\cdot)^H$ denote the conjugate, transpose, and Hermitian transpose. \odot and \otimes denote the Hadamard and Kronecker products. $\text{tr}(\cdot)$ and $\text{diag}(\cdot)$ return the trace and the main diagonal vector of a matrix. $\{\mathbf{X}_i\}_i$ is the set of \mathbf{X}_i for all i in its value range. $[\mathbf{X}]_i$ and $[\mathbf{X}]_{i,j}$ indicate the i -th row vector and the (i, j) -th element of \mathbf{X} . Besides, $[\mathbf{X}]_{i:j}$ is the sub-matrix of \mathbf{X} composed of its i -th to j -th row vectors. Moreover, \mathbf{I}_N denotes the N -dim unit matrix. $\mathbf{1}_N$ and \mathbf{J}_N denote all-ones N -dim vector and $N \times N$ matrix, respectively. $\Re(\cdot)$ is the real part of the argument.

II. SYSTEM MODEL

In this section, we introduce the MB RHS-based ISAC system. We describe its components, design a working protocol for it, and establish the channel model of the system.

A. System Components

As shown in Fig. 1, the system contains a BS equipped with a RHS serving multiple users in a region of interest (ROI). Each user has an omnidirectional antenna for Tx and Rx. The BS uses the RHS for receiving (Rx) and transmitting (Tx) orthogonal frequency division multiplexing (OFDM) signals for positioning and transmitting data, while it also has an omnidirectional antenna to broadcast beacons for link construction.

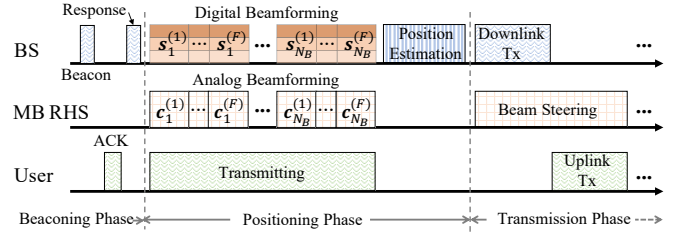


Fig. 2. Position-then-transmit protocol

The BS is connected to the RHS via K feeds, and each feed can send or receive signals from all the N_E meta-elements through on-board signal propagation. The N_E meta-elements are arranged as a square with the interval between adjacent meta-elements being Δ_E . Each meta-element can be electronically configured into multiple *states*, each with its own radiation coefficient. The radiation coefficients of all the meta-elements are referred to as the *configuration* of the RHS, which is denoted by vector $\mathbf{c} \in [0, 1]^{1 \times N_E}$ [3].

The RHS and BS are able to transmit and receive signals in N_B bands in a TDD manner by adjusting their configurations. Each band i ($i \in \{1, \dots, N_B\}$) is centered at frequency $f_{c,i}$ and composed of N_{SB} orthogonal sub-bands, each with center frequency $f_{i,j}$ ($j \in \{1, \dots, N_{SB}\}$) and bandwidth W . In each band, the BS is able to apply A&D beamforming. To be specific, the BS performs the analog beamforming by controlling the configuration \mathbf{c} of the RHS, and performs the digital beamforming through a weighted combination of the Tx/Rx symbols for different feeds, with combining vector denoted by $\mathbf{s} \in \mathbb{C}^{1 \times K}$. The A&D beamforming capability enables the BS to steer Tx/Rx beams, enhancing positioning and communication.

A user positioning process is performed by the BS processing the Rx signals from the users. The users are within the ROI, which is modeled as a 3D spatial region with dimensions $l_x \times l_y \times l_z$ m^3 and is rich in scatterers. The probability distribution of user position within the ROI is I^U , and the maximum speed of each user is v_{\max} . We assume that v_{\max} is not large and thus the users' positions can be considered fixed during each positioning process.

B. Protocol Design

We propose a position-then-transmit protocol to coordinate the system. As shown in Fig. 2, the protocol contains three phases, i.e., the *beaconing phase*, the *positioning phase*, and the *transmission phase*. In the beaconing phase, the BS broadcasts beacons for link construction. The users who want to communicate with the BS reply acknowledgement frames to the BS. The BS selects one of the users who have constructed an available link, responds to it, and proceeds to the next phase.

In the positioning phase, the selected user transmits signals to the BS through N_B bands sequentially, and the BS receives the signals for F frames in each band. Specifically, in the frame q ($q \in \{1, \dots, F\}$) of band i , the configuration of the RHS is $\mathbf{c}_i^{(q)}$, and the combining vector is $\mathbf{s}_{i,j}^{(q)}$ for sub-band j of band i . Besides, the combining vector of the BS is bound

by the maximum power P_{\max} . Denoting the received signals of the BS in sub-band j of band i over the F frames as vector $\mathbf{y}_{i,j} \in \mathbb{C}^{1 \times F}$, the received signals in this phase can be arranged as matrix $\mathbf{Y}_{\text{Rx}} \in \mathbb{C}^{N_{\text{B}} \times N_{\text{SB}} F}$, whose block-wise elements are $[\mathbf{Y}_{\text{Rx}}]_{i,j} = \mathbf{y}_{i,j}$. At the end of this phase, the BS uses a *positioning function* to estimate the position of the user, and the result is denoted by $\tilde{\mathbf{p}}^{\text{U}}$. Moreover, despite incurring additional overhead in this phase, it should be noted that the user's transmission can also be used for sensing purposes: A user can function as a monostatic radio-frequency sensor for the surrounding environment and motion [12]. In this regard, this phase can be integrated into a higher-level ISAC network, and the overhead can be justified.

In the transmission phase, the BS steers its beam to maximize the channel capacity towards $\tilde{\mathbf{p}}^{\text{U}}$. The BS and the user start downlink/uplink transmission over one of the N_{B} bands.

C. Channel Model

We establish the channel model by analyzing the equivalent base-band expression of the BS's received signals when a user at \mathbf{p}^{U} is transmitting. Without loss of generality, we model the received signal in sub-band j of band i at frame q . Based on [13], for meta-element m ($m \in \{1, \dots, N_{\text{E}}\}$), its received signal can be expressed as

$$\tau_{i,j,m}^{(q)} = (h_{i,j,m}^{\text{LoS}}(\mathbf{p}^{\text{U}}) + h_{i,j,m}^{\text{MP},(q)}) \cdot x, \quad (1)$$

where x indicates the Tx symbol of the user. Here, $h_{i,j,m}^{\text{LoS}}$ is the gain of the line-of-sight (LoS) path from the user at \mathbf{p}^{U} to the meta-element m , which can be expressed as

$$h_{i,j,m}^{\text{LoS}}(\mathbf{p}^{\text{U}}) = \frac{v_0 \cdot g_i^{\text{E}} \cdot g_i^{\text{U}} \cdot \exp(-\mathfrak{i} \frac{2\pi f_{i,j}}{v_0} \cdot \|\mathbf{p}^{\text{U}} - \mathbf{p}_m^{\text{E}}\|_2)}{4\pi f_{i,j} \cdot \|\mathbf{p}^{\text{U}} - \mathbf{p}_m^{\text{E}}\|_2},$$

where v_0 is the speed of light, \mathfrak{i} is the imaginary unit, g_i^{U} and g_i^{E} denote the gains of user's antenna and the meta-element, respectively, and \mathbf{p}_m^{E} is the position of meta-element m .

Besides, in (1), $h_{i,j,m}^{\text{MP},(q)}$ denotes the overall multipath gain. Based on the multi-path gain model for OFDM signals in rich-scattering environments [13], we can model $h_{i,j,m}^{\text{MP},(q)}$ as a complex random variable following wide-sense stable (WSS) Gaussian distribution. Specifically, denoting $\mathbf{h}_{i,j}^{\text{MP},(q)} = (h_{i,j,1}^{\text{MP},(q)}, \dots, h_{i,j,N_{\text{E}}}^{\text{MP},(q)})^{\text{T}}$ and with the help of [14], $\mathbf{h}_{i,j}^{\text{MP},(q)} \sim \mathcal{CN}(0, \mathbf{V}_i)$, where covariance matrix \mathbf{V}_i can be obtained by the expectation of the outer product of RHS's array response $\boldsymbol{\alpha}_i(\boldsymbol{\theta}) \in \mathbb{C}^{N_{\text{E}}}$ over the angular domain, i.e.,

$$\mathbf{V}_i = \mathbb{E}(\boldsymbol{\alpha}_i(\boldsymbol{\theta})\boldsymbol{\alpha}_i(\boldsymbol{\theta})^{\text{H}}) = \oint \boldsymbol{\alpha}_i(\boldsymbol{\theta})\boldsymbol{\alpha}_i(\boldsymbol{\theta})^{\text{H}} P_{\text{pap}}(\boldsymbol{\theta}) d\boldsymbol{\theta}, \quad (2)$$

where $[\boldsymbol{\alpha}_i(\boldsymbol{\theta})]_m = \exp(\mathfrak{i} \frac{2\pi f_{c,i}}{v_0} (\mathbf{p}_m^{\text{E}} - \mathbf{p}_1^{\text{E}}) \cdot \hat{\mathbf{n}}(\boldsymbol{\theta})) \cdot g_i^{\text{E}}$ with $\hat{\mathbf{n}}(\boldsymbol{\theta})$ being the unit normal vector for $\boldsymbol{\theta}$, and $P_{\text{pap}}(\boldsymbol{\theta})$ is the *power-angle profile* of the RHS. Based on [14], we model the covariance between the multi-path gains in the same band as

$$\mathbb{E} \left[\mathbf{h}_{i,j_1}^{\text{MP},(q_1)} (\mathbf{h}_{i,j_2}^{\text{MP},(q_2)})^{\text{H}} \right] = \rho_{f,i}(j_1, j_2) \cdot \rho_{t,i}(q_1, q_2) \cdot \mathbf{V}_i, \quad (3)$$

$$\rho_{f,i}(j_1, j_2) = (1 + \mathfrak{i} 2\pi \sigma_{\text{rms},i}(f_{i,j_1} - f_{i,j_2}))^{-1}, \quad (3)$$

$$\rho_{t,i}(q_1, q_2) = \mathcal{J}_0(2\pi f_{D,i}(q_1 - q_2)\Delta_t). \quad (4)$$

In (3), $\sigma_{\text{rms},i}$ indicates the *root mean square (rms) power*

delay spread of band i . In (4), \mathcal{J}_0 is the *zeroth-order Bessel function of the first kind*, $f_{D,i}$ indicates the maximum Doppler frequency, which can be calculated by $f_{D,i} = v_{\max} f_{c,i}/v_0$, and Δ_t denotes the time duration of a frame. We assume that different bands have larger spectral intervals than the coherence bandwidth of the channel, and thus the multi-path gains of different bands have zero covariance.

Then, based on (1), the received signal at feed k ($k \in \{1, \dots, K\}$) is

$$y_{i,j,k}^{(q)} = \sum_{m=1}^{N_{\text{E}}} \tau_{i,j,m}^{(q)} \cdot \kappa(f_{i,j}, \mathbf{p}_m^{\text{E}}, \mathbf{p}_k^{\text{F}}), \quad (5)$$

where $\kappa(f_{i,j}, \mathbf{p}_m^{\text{E}}, \mathbf{p}_k^{\text{F}})$ is the onboard propagation gain. Based on [3], it can be calculated as

$$\kappa(f, \mathbf{p}_s, \mathbf{p}_d) = \exp(-\mathfrak{i} \cdot \frac{2\pi n_{\text{r}} f}{v_0} \cdot \|\mathbf{p}_d - \mathbf{p}_s\|_2), \quad (6)$$

where n_{r} is the relative refractive index of the RHS board.

Combine the received signals at the K feeds with weight $\mathbf{s}_{i,j}^{(q)}$, and the received signal at the BS can be modeled as

$$\mathbf{y}_{i,j}^{(q)} = \sum_{k=1}^K \mathbf{s}_{i,j,k}^{(q)} y_{i,j,k}^{(q)} + e, \quad (7)$$

where $e \sim \mathcal{CN}(0, \sigma_n^2)$ is the thermal noise. Given power spectral density of noise being P_{N} , noise power $\sigma_n^2 = P_{\text{N}} W$.

Finally, based on (1), (5), and (7), the received signals in the positioning phase can be formulated into matrix form, i.e.,

$$[\mathbf{Y}_{\text{Rx}}]_i = \text{diag}((\mathbf{H}_i^{\text{LoS}}(\mathbf{p}^{\text{U}}) \otimes \mathbf{1}_F + \mathbf{H}_i^{\text{MP}}) \mathbf{T}_i^{\text{T}}) x + e, \quad (8)$$

where the elements of the above matrices can be expressed as

$$[\mathbf{H}_i^{\text{LoS}}(\mathbf{p}^{\text{U}})]_{j,m} = h_{i,j,m}^{\text{LoS}}(\mathbf{p}^{\text{U}}), [\mathbf{H}_i^{\text{MP}}]_{(q-1)N_{\text{SB}}+j,m} = h_{i,j,m}^{\text{MP},(q)},$$

$$[\mathbf{T}_i]_j = \mathbf{C}_i \odot (\mathbf{S}_{i,j} \mathbf{B}_{i,j}), [\mathbf{S}_{i,j}]_q = \mathbf{s}_{i,j}^{(q)}, \quad (9)$$

$$[\mathbf{C}_i]_q = \mathbf{c}_i^{(q)}, [\mathbf{B}_{i,j}]_{k,m} = \kappa(f_{i,j}, \mathbf{p}_m^{\text{E}}, \mathbf{p}_k^{\text{F}}).$$

Based on channel reciprocity, when the BS transmits, the received signals at the user can also be calculated by (8).

Furthermore, we model the channel capacity in the transmission phase of band i given unit symbol. Assuming that the BS adopts combining vectors $\hat{\mathbf{s}}_{i,1}, \dots, \hat{\mathbf{s}}_{i,N_{\text{SB}}}$ and RHS configuration $\hat{\mathbf{c}}_i$, the channel capacity of the band i can be calculated by

$$R_i = \sum_{j=1}^{N_{\text{SB}}} W \log_2 \left(1 + \frac{\|\hat{\mathbf{t}}_{i,j} [\mathbf{H}_i^{\text{LoS}}(\mathbf{p}^{\text{U}})]_j\|_2^2 + \hat{\mathbf{t}}_{i,j} \mathbf{V}_i \hat{\mathbf{t}}_{i,j}^{\text{H}}}{\sigma_n^2} \right), \quad (10)$$

where the received signal power of both the LoS and the multi-path channels are considered, and $\hat{\mathbf{t}}_{i,j} = \hat{\mathbf{c}}_i \odot \hat{\mathbf{s}}_{i,j} \mathbf{B}_{i,j}$.

III. PROBLEM FORMULATION

In this section, we formulate the A&D beamforming optimization problem of the MB RHS-based ISAC system.

As in [15], we adopt the average CRLB in the ROI to evaluate the system's positioning performance, which indicates the lower-bound of the mean square error (MSE) of positioning. Given the A&D beamforming of the RHS, the CRLB for the system to position a user at \mathbf{p}^{U} can be derived by Proposition 1.

Proposition 1. *The CRLB for MB RHS-based ISAC system to position a user at $\mathbf{p}^U \in \mathbb{R}^{1 \times 3}$ can be calculated by*

$$\text{CRLB}(\mathbf{p}^U) = \sum_{u=1}^3 [\mathbf{I}_{\text{FIM}}^{-1}(\mathbf{p}^U)]_{uu}. \quad (11)$$

Here, $\mathbf{I}_{\text{FIM}}(\mathbf{p}^U) \in \mathbb{R}^{3 \times 3}$ is the Fisher information matrix (FIM) of \mathbf{Y}_{Rx} w.r.t. \mathbf{p}^U , whose element can be calculated as:

$$[\mathbf{I}_{\text{FIM}}(\mathbf{p}^U)]_{u,v} = 2\Re \left(\sum_{i=1}^{N_B} \left(\frac{\partial \hat{\mathbf{y}}_i}{\partial p_u^U} \right)^H \mathbf{A}_i^{-1} \left(\frac{\partial \hat{\mathbf{y}}_i}{\partial p_v^U} \right) \right), \quad (12)$$

$$\frac{\partial \hat{\mathbf{y}}_i}{\partial p_u^U} = \text{diag} \left((\dot{\mathbf{H}}_{i,u}^{\text{LoS}} \otimes \mathbf{1}_F) \mathbf{T}_i^T \right), \quad \dot{\mathbf{H}}_{i,u}^{\text{LoS}} = \frac{\partial \mathbf{H}_i^{\text{LoS}}}{\partial p_u^U}, \quad (13)$$

$$\mathbf{A}_i = (\mathbf{K}_{f,i} \otimes \mathbf{J}_F) \odot (\mathbf{J}_{N_{\text{SB}}} \otimes \mathbf{K}_{t,i}) \odot (\mathbf{T}_i \mathbf{V}_i \mathbf{T}_i^H) + \sigma_n^2 \mathbf{I}, \quad (14)$$

$$[\mathbf{K}_{f,i}]_{j_1, j_2} = \rho_{f,i}(j_1, j_2), \quad [\mathbf{K}_{t,i}]_{q_1, q_2} = \rho_{t,i}(q_1, q_2). \quad (15)$$

Proof: The FIM in (12) can be obtained by substituting the channel model in (8) into the FIM Eq. (6.55) in [16], and the CRLB can be derived based on Eq. (27) in [7]. ■

Then, the A&D beamforming optimization problem of the system for CRLB minimization can be formulated as:

$$(P1) : \min_{\{\mathbf{S}_{i,j}\}_{i,j}, \{\mathbf{C}_i\}_i} \mathbb{E}_{\mathbf{p}^U \in \Gamma^U} (\text{CRLB}(\mathbf{p}^U)), \quad (16a)$$

$$\text{s.t.} \quad (9) \sim (15), \quad (16b)$$

$$\sum_{j=1}^{N_{\text{SB}}} (\mathbf{s}_{i,j}^{(q)})^H \mathbf{s}_{i,j}^{(q)} = P_{\max}, \quad (16c)$$

$$\mathbf{0} \preceq \mathbf{C}_i \preceq \mathbf{1}. \quad (16d)$$

The challenges in solving (P1) lie in the following aspects. *Firstly*, due to the non-convex relationship between $\{\mathbf{S}_{i,j}\}_{i,j}$, $\{\mathbf{C}_i\}_i$ and the CRLB, (P1) is non-convex and NP-hard. *Secondly*, the objective function (16a) is of high computational cost since it is calculated over the ROI. *Thirdly*, as multiple bands are used, the number of variables can be very large, i.e., $N_B F(N_{\text{SB}}K + N_E)$, which makes it hard for conventional algorithms to handle efficiently. Therefore, it is necessary to design novel algorithm to solve (P1) efficiently.

IV. ALTERNATING ANALOG AND DIGITAL BEAMFORMING OPTIMIZATION ALGORITHM

In this section, we propose an efficient algorithm named *alternating A&D beamforming optimization algorithm* to solve (P1). *Firstly*, to avoid the high complexity in finding the global optimum of a non-convex problem, we focus on gradient-based methods to search for a local optimum. *Secondly*, to reduce the complexity in calculating (16a), we adopt the Monte Carlo method to sample the ROI. *Thirdly*, to handle the large number of variables, we alternately optimize A&D beamforming variables and derive the gradient formulas of the CRLB in a matrix form that is easy to calculate.

The ROI is sampled following distribution Γ^U , and N_{sam} sampled positions are obtained and denoted by set \mathcal{S}_{sam} . Then, (16a) is converted into:

$$\min_{\{\mathbf{S}_{i,j}\}_{i,j}, \{\mathbf{C}_i\}_i} \sum_{\mathbf{p}^U \in \mathcal{S}_{\text{sam}}} \frac{\text{CRLB}(\mathbf{p}^U)}{N_{\text{sam}}}. \quad (17)$$

We then solve the above problem by alternately optimizing $\{\mathbf{C}_i\}_i$ and $\{\mathbf{S}_{i,j}\}_{i,j}$ in an iterative manner. In the ρ -th iteration, $\{\mathbf{C}_i\}_i$ is optimized given $\{\mathbf{S}_{i,j}\}_{i,j}^{(\rho-1)}$ by solving (sP1):

$$(sP1) : \min_{\{\mathbf{C}_i\}_i} \sum_{\mathbf{p}^U \in \mathcal{S}_{\text{sam}}} \frac{\text{CRLB}(\mathbf{p}^U)}{N_{\text{sam}}}, \text{ s.t. } (9) \sim (15), (16d).$$

To solve (sP1) efficiently, we derive the gradient formulas of the objective average CRLB in Proposition 2.

Proposition 2. *The gradient of the average CRLB w.r.t. \mathbf{C}_i can be calculated as:*

$$\sum_{\mathbf{p}^U \in \mathcal{S}_{\text{sam}}} \frac{\partial \text{CRLB}(\mathbf{p}^U)}{\partial \mathbf{C}_i} = - \sum_{\mathbf{p}^U \in \mathcal{S}_{\text{sam}}} \text{tr} \left(\frac{\partial \mathbf{I}_{\text{FIM}}(\mathbf{p}^U)}{\partial \mathbf{C}_i} \mathbf{I}_{\text{FIM}}^{-2}(\mathbf{p}^U) \right),$$

$$\left[\frac{\partial \mathbf{I}_{\text{FIM}}(\mathbf{p}^U)}{\partial \mathbf{C}_i} \right]_{u,v} = \mathbf{A}_{i,vu}^c + \mathbf{A}_{i,uv}^c + \mathbf{B}_{i,uv}^c + \mathbf{B}_{i,vu}^c,$$

where $u, v \in \{1, 2, 3\}$. The detailed expressions of $\mathbf{A}_{i,uv}^c$ and $\mathbf{B}_{i,uv}^c$ can be found in Appendix A.

Proof: The gradient is obtained by calculating the partial derivatives of (11) w.r.t. \mathbf{C}_i , based on (36)~(40) in [17]. ■

Based on Proposition 2, (sP1) is solved by updating $\{\mathbf{C}_i\}_i$ along the inverse direction of the gradient. As for the constraints in (sP1), constraints (9)~(15) are implicitly contained in the calculation of gradients. Besides, constraint (16d) can be handled by the *interior point approach*, where a barrier function is used to restrict $\{\mathbf{C}_i\}_i$ within its feasible region [18]. Moreover, we adopt *conjugate gradient (CG) method* to calculate the update by solving a quadratic approximation of (sP1) within a local region of current $\{\mathbf{C}_i\}_i$ [18]. The result of solving (sP1) in the ρ -th iteration is denoted by $\{\mathbf{C}_i\}_i^{(\rho)}$.

Given $\{\mathbf{C}_i\}_i^{(\rho)}$, $\{\mathbf{S}_{i,j}\}_{i,j}$ is optimized by solving (sP2):

$$(sP2) : \min_{\{\mathbf{S}_{i,j}\}_{i,j}} \sum_{\mathbf{p}^U \in \mathcal{S}_{\text{sam}}} \frac{\text{CRLB}(\mathbf{p}^U)}{N_{\text{sam}}}, \text{ s.t. } (9) \sim (15), (16c).$$

Similar with solving (sP1), we adopt gradient-based method to solve (sP2), where the gradient is derived in Proposition 3.

Proposition 3. *The gradient of the average CRLB w.r.t. $\mathbf{S}_{i,j}$ can be calculated as*

$$\sum_{\mathbf{p}^U \in \mathcal{S}_{\text{sam}}} \frac{\partial \text{CRLB}(\mathbf{p}^U)}{\partial \mathbf{S}_{i,j}} = - \sum_{\mathbf{p}^U \in \mathcal{S}_{\text{sam}}} \text{tr} \left(\frac{\partial \mathbf{I}_{\text{FIM}}(\mathbf{p}^U)}{\partial \mathbf{S}_{i,j}} \mathbf{I}_{\text{FIM}}^{-2}(\mathbf{p}^U) \right),$$

$$\left[\frac{\partial \mathbf{I}_{\text{FIM}}(\mathbf{p}^U)}{\partial \mathbf{S}_{i,j}} \right]_{u,v} = \mathbf{A}_{i,j,vu}^s + \mathbf{A}_{i,j,uv}^s + \mathbf{B}_{i,j,uv}^s + \mathbf{B}_{i,j,vu}^s,$$

where $u, v \in \{1, 2, 3\}$. The detailed expressions of $\mathbf{A}_{i,j,uv}^s$ and $\mathbf{B}_{i,j,uv}^s$ can be found in Appendix A.

Proof: The gradient is obtained by calculating partial derivatives of (11) w.r.t. $\mathbf{S}_{i,j}$, based on (36)~(40) in [17]. ■

We solve (sP2) also by gradually updating each $\{\mathbf{S}_{i,j}\}_{i,j}$ along the inverse direction of its gradient, and the interior point approach is used to handle constraint (16c) with CG method utilized to calculate the update. The result of solving (sP2) in the ρ -th iteration is denoted by $\{\mathbf{S}_{i,j}\}_{i,j}^{(\rho)}$.

Within each iteration, the number of update steps for $\{\mathbf{C}_i\}_i$ and $\{\mathbf{S}_{i,j}\}_{i,j}$ are denoted by N_{us} . The iteration process terminates when the results are not changed by the last update

Algorithm 1 Alternating Analog and Digital Beamforming Optimization Algorithm

- 1: Sample N_{sam} positions following Γ^U and obtain \mathcal{S}_{sam} .
 - 2: Set initial points by $\{\mathcal{S}_{i,j}\}_{i,j}^{(0)} = \{\mathcal{S}_{i,j} | \mathbf{s}_{i,j}^{(q)} = \mathbf{1} \cdot \sqrt{P_{\text{max}}/K}\}$ and $\{\mathcal{C}_i\}_i^{(0)}$ with elements randomly chosen from $[0, 1]$.
 - 3: **for** $\rho = 1, \dots, N_{\text{itr}}$ **do**
 - 4: Given $\{\mathcal{S}_{i,j}\}_{i,j}^{(\rho-1)}$ and $\{\mathcal{C}_i\}_i^{(\rho-1)}$, solve (sP1) to obtain $\{\mathcal{C}_i\}_i^{(\rho)}$ using the gradient formula in Proposition 2.
 - 5: Given $\{\mathcal{C}_i\}_i^{(\rho)}$ and $\{\mathcal{S}_{i,j}\}_{i,j}^{(\rho-1)}$, solve (sP2) to obtain $\{\mathcal{S}_{i,j}\}_{i,j}^{(\rho)}$ using the gradient formula in Proposition 3.
 - 6: **If** $\{\mathcal{S}_{i,j}\}_{i,j}^{(\rho-1)} = \{\mathcal{S}_{i,j}\}_{i,j}^{(\rho)}$ and $\{\mathcal{C}_i\}_i^{(\rho-1)} = \{\mathcal{C}_i\}_i^{(\rho)}$: **break**
 - 7: **end for**
 - 8: **return** $\{\mathcal{S}_{i,j}\}_{i,j}^* = \{\mathcal{S}_{i,j}\}_{i,j}^{(\rho)}$ and $\{\mathcal{C}_i\}_i^* = \{\mathcal{C}_i\}_i^{(\rho)}$.
-

TABLE I
SIMULATION PARAMETERS

Parameter	Value	Parameter	Value
N_B	2	N_E	10×10
K	3	$\sigma_{\text{rms},i}$	$0.5 \mu\text{s}$
N_{SB}	8	v_{max}	20 km/h
Δ_t	$4 \mu\text{s}$	P_N	-174 dBm/Hz
F	4	P_{max}	1 mW
W	125 kHz	N_{sam}	1200
N_{us}	50	N_{itr}	4

or when the number of iterations exceeds N_{itr} . The complete algorithm is summarized as Algorithm 1.

V. SIMULATION RESULTS

In this section, we present the simulation setup and the key results. We establish a 3D coordinate system with its origin at the center of RHS, its x-axis along the perpendicular direction of RHS, and its z-axis pointing vertically upward. The ROI is a cuboid region centering at (10, 0, 0) m and has dimensions (10, 10, 2) m. The distribution of users' positions, i.e. Γ^U , is a 3D uniform distribution within the ROI. The gains of each meta-element and user's antenna are $g_i^E = g_i^U = 1$, while it is worth noticing that the proposed system and algorithm can adapt to meta-elements with other patterns of gain.

Moreover, the RHS board in the simulation is made of FR-4, which is a typical dielectric material used for printed circuit boards and has $n_r = 2.1$. The N_B bands of the system are centered at $(2 + 0.5i)$ GHz with a 500 MHz interval, and the average wavelength of the center frequencies is denoted by λ_{avr} . The interval between adjacent meta-elements is set to be $0.3\lambda_{\text{avr}}$. Besides, based on [14], $P_{\text{pap}}(\theta)$ in (2) is modeled as a Laplacian function with zero mean and angular spread 10° in both azimuth and elevation, scaled by the average LoS power within the ROI. The other parameters are listed in Table I.

Firstly, we show the effectiveness of the proposed algorithm in terms of CRLB minimization and the computational efficiency. We compare it with two benchmark algorithms:

- **Direct Gradient Descent:** Problem (P1) is solved by using gradient descent directly without alternating variables. Gradients are calculated based on the Propositions 2 and 3. For a fair comparison, the total number of update steps is set to $2 \times N_{\text{itr}} \times N_{\text{us}}$, and the interior point approach with CG

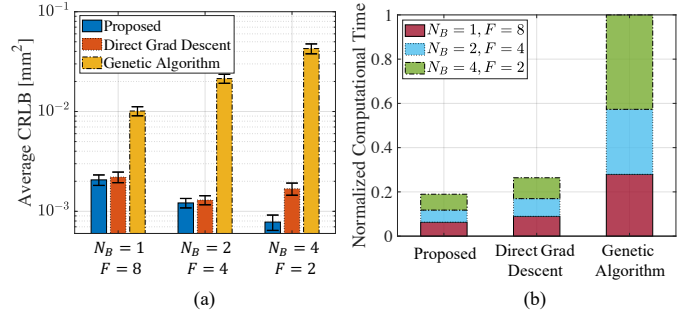


Fig. 3. Average optimization results of (a) CRLB and (b) computational time of the proposed and benchmark algorithms. N_{sam} is set to 10 ensure fast output, and 30 independent trails are performed to reduce the impact of sampling randomness. The length of the “T”-shaped bars in (a) represents the standard deviations of the results.

method is also adopted.

- **Genetic Algorithm:** The genetic algorithm is employed as in [19], which minimizes the CRLB by optimizing $\{\mathcal{S}_{i,j}\}_{i,j}$ and $\{\mathcal{C}_i\}_i$ jointly. The standard Matlab implementation is adopted with the maximum number of generations set to 10.

Figs. 3 (a) and (b) show the comparison results of the resulting CRLB and the normalized computational time for the proposed and benchmark algorithms, respectively. It can be observed that the proposed algorithm results in lower CRLB values and takes less computational time compared with the benchmark algorithms. Fig. 3 (a) also shows that the resulting CRLB of the proposed algorithm decreases with N_B given fixed $N_B F$, which proves the effectiveness of using MB technique. Moreover, the CRLB gap between the proposed algorithm and the benchmarks increases with N_B . This implies that the advantage of the proposed algorithm becomes more pronounced as N_B increases.

Secondly, we show the effectiveness of the optimized A&D beamforming in terms of its resulting positioning precision and its benefit for the communication capacity. We compare the optimized A&D beamforming with two benchmark beamforming used in [15]:

- **Directional:** The A&D beamforming is designed to generate focused beams scanning the ROI during the frames in the positioning phase.
- **Random:** Elements of $\{\mathcal{C}_i\}_i$ follow a uniform distribution in range $[0, 1]$, and elements of $\{\mathcal{S}_{i,j}\}_{i,j}$ take uniform values that satisfy the power constraint.

Figs. 4 (a) and (b) show the violin plot and the box plot comparing the performance of different beamformings in terms of the MSE of positioning and the communication capacity loss due to positioning errors, respectively of 256 nodes. Specifically, in Fig. 4 (a), the MSE of positioning is evaluated by the training result of a neural network with a single hidden-layer. The neural networks in different cases are trained by datasets each containing 10^5 pairs of simulated received signals and position labels obtained by the system with different beamforming. During the training, the division between training, validation, and test data follows ratio 7:1.5:1.5. It can be observed in Fig. 4 (a) that, on average, by using

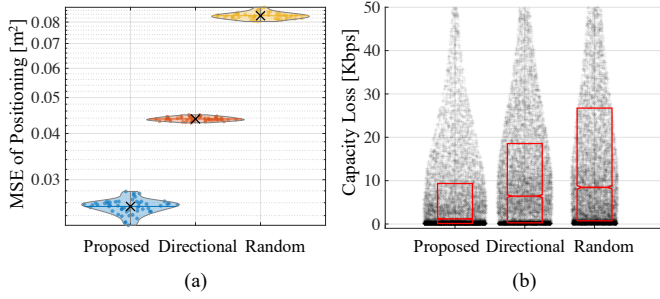


Fig. 4. (a) MSE of positioning and (b) communication capacity loss due to positioning error given different A&D beamforming. In (a), 50 independent training are conducted for the neural network. Each dot represents the result of a single trial, the filled regions indicate the overall distribution of the results, and “x” represents the mean value. In (b), the best training result of each case is used, and 1000 random positions are sampled. The translucent background figures indicate the patterns of the capacity loss of individual samples. The red boxplots show the distribution of the results, with the bottom, middle, and top lines indicating the 25th, 50th, and 75th percentiles, respectively.

the optimized A&D beamforming, the system reduces MSE of positioning by 42% and 69%, compared to the Directional and Random beamforming benchmarks.

Besides, in Fig. 4 (b), the communication capacity loss is evaluated by the difference between the capacity of band 1 when the BS steers its beam towards user’s true position and that when the beam is steered towards the estimated position. It can be observed that the optimized A&D beamforming results in 82% and 86% reduction in median levels of capacity loss, compared with Directional and Random benchmarks, respectively. Moreover, the interquartile range, i.e., the range between 25% and 75% levels, of the capacity loss is also significantly reduced by the proposed algorithm, which are 50% and 64% lower than those of the benchmarks.

VI. CONCLUSION

In this paper, we have proposed the MB RHS-based ISAC system. We have designed the position-then-transmit protocol, established the channel model, and analyzed the CRLB of the system. Then, we have designed an A&D beamforming optimization algorithm for the CRLB minimization, which handles the large number of beamforming variables efficiently. Simulation results have shown that firstly, the proposed algorithm achieves lower average CRLB with less computational time compared with benchmark algorithms. Secondly, the A&D beamforming obtained by the proposed algorithm results in 42% lower MSE of positioning, which leads to 82% less communication capacity loss, compared with the benchmark directional beamforming.

APPENDIX A

With the help of [17], $\mathbf{A}_{i,uv}^c$, $\mathbf{B}_{i,uv}^c$, $\mathbf{A}_{i,j,uv}^s$, and $\mathbf{B}_{i,j,uv}^s$ ($\forall u, v \in \{1, 2, 3\}$) can be derived as

$$\begin{aligned} \mathbf{A}_{i,uv}^c &= 2\Re\left(\sum_{j=1}^{N_{\text{SB}}}([\bar{\zeta}_{i,u}]_{(j-1)F+1:jF} \otimes \mathbf{1}_{N_{\text{E}}}^{\top})\right. \\ &\quad \left.\odot [\dot{\mathbf{H}}_{i,v}^{\text{LoS}}]_{(j-1)F+1:jF} \odot (\mathbf{S}_{i,j} \mathbf{B}_{i,j})\right), \\ \mathbf{B}_{i,uv}^c &= -2\Re\left(\sum_j^{N_{\text{SB}}}([\bar{\zeta}_{i,u}]_{(j-1)F+1:jF} \otimes \mathbf{1}_{N_{\text{E}}}^{\top}) \odot (\mathbf{S}_{i,j} \mathbf{B}_{i,j})\right) \end{aligned}$$

$$\begin{aligned} &\odot \mathbf{R}_{F \times N_{\text{E}}}([\mathbf{K}_{\text{ft},i}]_{(j-1)F+1:jF} \odot ((\mathbf{V}_i \mathbf{T}_i^{\text{H}}) \otimes \mathbf{1}_F) \zeta_{i,v}), \\ \mathbf{A}_{i,j,uv}^s &= 2\Re([\bar{\zeta}_{i,u}]_{(j-1)F+1:jF} \otimes \mathbf{1}_K^{\top} \\ &\quad \odot \mathbf{R}_{F \times K}([\dot{\mathbf{H}}_{i,v}^{\text{LoS}}]_{(j-1)F+1:jF} \odot \mathbf{C}_i) \odot (\mathbf{B}_{i,j} \otimes \mathbf{1}_F) \mathbf{1}_{N_{\text{E}}}), \\ \mathbf{B}_{i,j,uv}^s &= -2\Re([\bar{\zeta}_{i,u}]_{(j-1)F+1:jF} \otimes \mathbf{1}_K^{\top}) \\ &\quad \odot \mathbf{R}_{F \times K}([\mathbf{K}_{\text{ft},i}]_{(j-1)F+1:jF} \odot ((\mathbf{C}_i \odot \mathbf{B}_{i,j} \otimes \mathbf{1}_F) (\mathbf{V}_i \mathbf{T}_i^{\text{H}}))) \zeta_{i,v}), \end{aligned}$$

where $\zeta_{i,u} = \Lambda_i^{-1}(\dot{\mathbf{H}}_{i,u}^{\text{LoS}} \odot \mathbf{T}_i) \mathbf{1}_{N_{\text{E}}} \in \mathbb{C}^{N_{\text{SB}}F \times 1}$, operator \odot denotes the *penetrating face product*, $\mathbf{K}_{\text{ft},i} = (\mathbf{K}_{\text{f},i} \otimes \mathbf{J}_F) \odot (\mathbf{J}_{N_{\text{SB}}} \otimes \mathbf{K}_{\text{t},i})$, and $\mathbf{R}_{F \times K}(\cdot)$ reshapes the argument into a $F \times K$ matrix.

REFERENCES

- [1] R. Deng, B. Di, H. Zhang, D. Niyato, Z. Han, H. V. Poor, and L. Song, “Reconfigurable holographic surfaces for future wireless communications,” *IEEE Wireless Commun.*, vol. 28, no. 6, pp. 126–131, Dec. 2021.
- [2] M. Boyarsky, T. Slesman, M. F. Imani, J. N. Gollub, and D. R. Smith, “Electronically steered metasurface antenna,” *Sci. Rep.*, vol. 11, no. 1, pp. 1–10, Feb. 2021.
- [3] H. Zhang, H. Zhang, B. Di, M. D. Renzo, Z. Han, H. V. Poor, and L. Song, “Holographic integrated sensing and communication,” *IEEE J. Sel. Areas Commun.*, vol. 40, no. 7, pp. 2114–2130, Jul. 2022.
- [4] X. Wei, D. Shen, and L. Dai, “Channel estimation for RIS assisted wireless communications—Part I: Fundamentals, solutions, and future opportunities,” *IEEE Commun. Lett.*, vol. 25, no. 5, pp. 1398–1402, May 2021.
- [5] X. Zhang, H. Zhang, H. Zhang, and B. Di, “Holographic radar: Target detection enabled by reconfigurable holographic surfaces,” *IEEE Commun. Lett.*, Sep. 2022, early access.
- [6] H. Zhang, H. Zhang, B. Di, K. Bian, Z. Han, and L. Song, “Towards ubiquitous positioning by leveraging reconfigurable intelligent surface,” *IEEE Commun. Lett.*, vol. 25, no. 1, pp. 284–288, Jan. 2021.
- [7] A. Elzanaty, A. Guerra, F. Guidi, and M.-S. Alouini, “Reconfigurable intelligent surfaces for localization: Position and orientation error bounds,” *IEEE Trans. Signal Process.*, vol. 69, pp. 5386–5402, Aug. 2021.
- [8] C. Sturm, E. Pancera, T. Zwick, and W. Wiesbeck, “A novel approach to OFDM radar processing,” in *Proc. IEEE Radar Conf.*, Pasadena, CA, May 2009.
- [9] T. Ma, Y. Xiao, X. Lei, W. Xiong, and Y. Ding, “Indoor localization with reconfigurable intelligent surface,” *IEEE Commun. Lett.*, vol. 25, no. 1, pp. 161–165, Jan. 2021.
- [10] A. Jafari, L. Petrillo, J. Sarrazin, D. Lautru, P. De Doncker, and A. Benlarbi-Delai, “TDOA estimation method using 60 GHz OFDM spectrum,” *Int. J. Microwave Wireless Technol.*, vol. 7, no. 1, pp. 31–35, Feb. 2015.
- [11] A. B. Jagadeesan, A. Alphones, M. F. Karim, and L. Ong, “Metamaterial based reconfigurable multiband antenna,” in *Proc. IEEE APS/URSI*, Vancouver, BC, Canada, Jul. 2015.
- [12] Z. Chen, T. Zheng, C. Hu, H. Cao, Y. Yang, H. Jiang, and J. Luo, “ISACoT: Integrating sensing with data traffic for ubiquitous IoT devices,” *IEEE Commun. Mag.*, vol. 61, no. 3, pp. 1–7, Mar. 2022.
- [13] A. Goldsmith, *Wireless communications*. New York, USA: Cambridge university press, 2005.
- [14] G. Barriac and U. Madhow, “Space-time precoding for mean and covariance feedback: application to wideband OFDM,” *IEEE Trans. Commun.*, vol. 54, no. 1, pp. 96–107, Jan. 2006.
- [15] Z. Abu-Shaban, K. Keykhosravi, M. F. Keskin, G. C. Alexandropoulos, G. Seco-Granados, and H. Wymeersch, “Near-field localization with a reconfigurable intelligent surface acting as lens,” in *Proc. IEEE ICC*, Montreal, QC, Canada, Jun. 2021.
- [16] P. J. Schreier and L. L. Scharf, *Statistical signal processing of complex-valued data: the theory of improper and noncircular signals*. Cambridge, UK: Cambridge university press, 2010.
- [17] K. B. Petersen, M. S. Pedersen *et al.*, “The matrix cookbook,” *Tech. Univ. Denmark*, vol. 7, no. 15, p. 510, Nov. 2012.
- [18] R. H. Byrd, J. C. Gilbert, and J. Nocedal, “A trust region method based on interior point techniques for nonlinear programming,” *Math Program.*, vol. 89, no. 1, pp. 149–185, Nov. 2000.
- [19] C. L. Nguyen, O. Georgiou, and G. Gradoni, “Reconfigurable intelligent surfaces and machine learning for wireless fingerprinting localization,” *arXiv preprint arXiv:2010.03251*, 2020.